LA-UR-18-22140
Approved for public release; distribution is unlimited.

Title: Mesoscale anisotropic residual stress in additively manufactured Ti-6Al-4V

Author(s): Strantza, Maria
Vrancken, Bey
Prime, Michael Bruce
Truman, Chris
Rombouts, Marleen
Guillaume, Patrick
Van Hemelrijck, Danny

Intended for: Acta Materialia

Issued: 2018-03-13 (Draft)

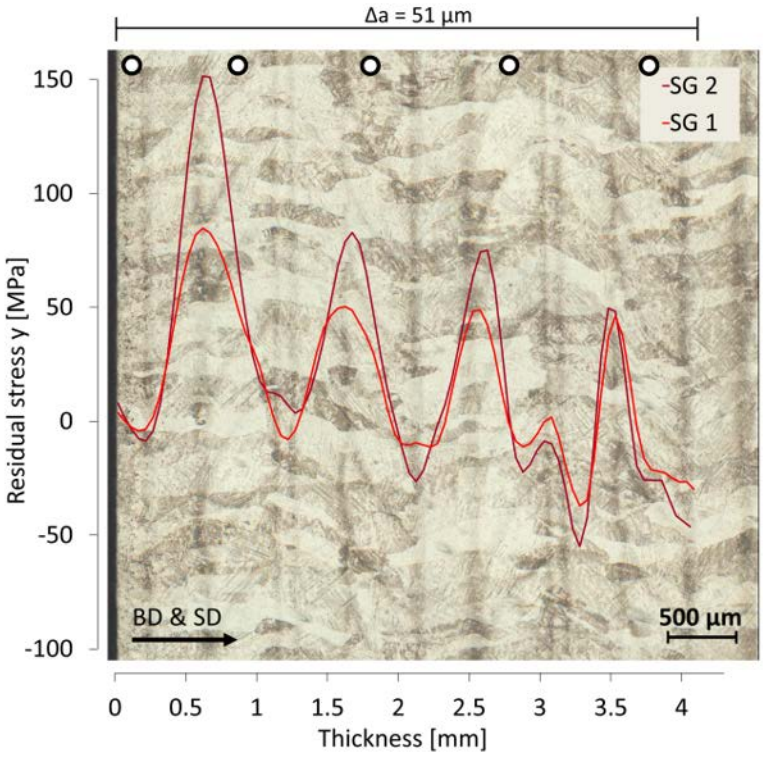

Final reference:

Strantza, M., Vrancken, B., Prime, M. B., Truman, C., Rombouts, M., Brown, D. W., Guillaume, P., and Van Hemelrijck, D., 2019, "Directional and oscillating residual stress on the mesoscale in additively manufactured Ti-6Al-4V," Acta Materialia, 168, pp. 299-308.

https://doi.org/10.1016/j.actamat.2019.01.050

Directional and oscillating residual stress on the mesoscale in additively manufactured Ti-6Al-4V

M. Strantza[a*, former b], B. Vrancken[c, former d], M. B. Prime[a], C. Truman[e], M. Rombouts[f],

D. W. Brown[a], P. Guillaume[g], D. Van Hemelrijck[b]

[a] Los Alamos National Laboratory, Los Alamos, New Mexico, US
[b] Department of Mechanics of Materials and Constructions, Vrije Universiteit Brussel, Brussels, Belgium
[c] Lawrence Livermore National Laboratory, Livermore, California, US
[d] Department of Materials Engineering, KU Leuven, Leuven, Belgium
[e] Department of Mechanical Engineering, University of Bristol, Bristol, UK
[f] Vlaamse Instelling voor Technologisch Onderzoek (VITO), Mol, Belgium
[g] Department of Mechanical Engineering, Vrije Universiteit Brussel, Brussels, Belgium

Abstract: In additive manufacturing of metals as compared to conventional processing, the directional track-by-track and layer-by-layer nature of the fabrication process can lead to residual stresses that locally are both directionally and spatially heterogeneous. Much of the existing literature has focused either on the macroscale residual stress inside the entire part, or on the microscale residual stresses that are created around a scan vector, thereby neglecting the intermediate length-scale of the different layers. The objective of this research is to investigate such mesoscale residual stress distributions across several layers in Ti-6Al-4V components produced by laser metal deposition process. The incremental centre hole drilling and incremental slitting methods provide measurements with excellent spatial resolution within and across the layer length scale. In this work, the two methods complemented each other to quantify both mesoscale and directional variations of residual stress that correlate with the deposition pattern. Our findings also provide strong evidence that an oscillatory residual stress variation persists even after thermal cycling that occurs during deposition of subsequent layers.

Keywords: Residual stress; intralayer; oscillatory variation; additive manufacturing; incremental centre hole drilling; incremental slitting.

1. Introduction

Laser metal deposition (LMD) –classified in the ASTM 2792-12a standard as a "directed energy deposition" or DED technique [1]– is one of the main additive manufacturing (AM) processes to produce complex metallic structures. During LMD, the small scale of the melt pool compared to the part dimensions leads to high thermal gradients. The thermal history that

*Corresponding author e-mail address: maria.strantza@lanl.gov; postal address: Los Alamos National Laboratory, MST-8, mailstop H805, Los Alamos, NM 87545, USA; phone number: +1 505 667 9576

the material goes through due to the track-by-track and layer-by-layer nature of the process causes unique residual stress (RS) distributions [2],[3]. According to Mercelis and Kruth [4], two main mechanisms have been proposed to contribute to RS in metallic AM. The first mechanism is the temperature gradient mechanism (TGM). The TGM mechanism does not include the liquid and is a solid state phenomenon that is exploited in laser forming [5], but is detrimental in AM. The TGM mechanism is a result of the rapid temperature gradient development caused by the laser spot, the heating and cooling of the solid material around the melt pool and the localized plastic deformation of that material. During the deposition, the local increase in temperature reduces the strength of the material. The hot material wants to expand but it is constrained by the surrounding material, leading to plastic compression. After subsequent cooling, the total shrinkage experienced will be larger for the plastically compressed material, leading to tensile stresses in the previously hot material at the surface. The second mechanism is associated with the addition, solidification, and thermal shrinkage of the melt pool. Both mechanisms contribute to a residual stress state consisting of tension at the top surface, balanced by compression below [4].

Several studies have been performed on LMD components (mainly in thin wall components) which linked the macroscale RS distribution with geometrical features and process parameters [3,6–11]. Pratt *et al.* [12] concluded that the scanning speed does not significantly affect the magnitude of the stresses, while internal stresses are slightly increased with increasing laser power. As early as 1999, Nickel *et al.* [13] studied the effect of the deposition patterns on RS, highlighting that distortions and thus stresses are greater in the direction of the deposition tracks. Griffith *et al.* [14] used holographic hole drilling in a hollow H13 tool steel box made by LENS. Measurements performed on a thin wall revealed tensile stresses in both horizontal and vertical direction along the vertical edges, as well as horizontal tensile stresses and compressive vertical stresses in the middle part of the wall. Additionally, RS measurements

using the hole drilling method on LMD components in Ref. [15] demonstrated that the stresses in the deposited material are lower than those in the substrate regions. In general, the literature indicates that residual stresses in LMD components are largest in the build direction. Tensile stresses on the outer surfaces are balanced by compressive stresses in the centre of the part [16], while the magnitude of the stress increases with increasing number of deposited layers [17]. To date, RS characterization of AM parts was mainly focused either on the macroscale distribution [18–20], or on the effect of orientation and length of scan vectors within one layer [21,22]. To the author's best knowledge, there are no studies in the literature which have investigated stress variations within a layer. Stress variations over the layer length scale are also important and sufficient to affect fatigue crack growth rates, for example, and therefore the life of a structural part.

In this work, we present novel results specific to *mesoscale* residual stress variations in AM Ti-6Al-4V parts produced by the LMD process. Residual stresses are customarily divided into three types depending on the length scale over which they vary continuously and equilibrate [23]. Type I, or macrostresses, vary over the dimensions of a part, typically mm or larger. Type II, also known as microstresses or intergranular stresses, vary from grain to grain in a polycrystal, typically on the order of 10's of μm. Type III, subgrain or atomic scale stresses, vary over sub-micron dimensions. Type II and especially type III stresses are often considered unimportant for life assessment of metallic components [24]. The type I-III length scale classification still holds for AM parts, but AM processes introduce an additional important length scale called the mesoscale corresponding to the characteristic length scale of the build layer thickness. We present results at the scale of build layer thickness, which lengthwise is between type I and II scales although the process-based cause makes these mesoscale stresses physically more similar to macrostresses.

Incremental centre hole drilling (ICHD) [25–27] and the slitting method [28–30] are two residual stress measurement techniques that are widely known to both academia and industry. These methods are particularly suited to capture in-plane directional residual stresses and the mesoscale gradient therein over the range of several layers. In contrast, diffraction based techniques tend to focus on macroscale residual stresses [31], which are inaccessible to ICHD and struggle with the mesoscale because a proper statistical sampling of grains is difficult to achieve. In this work, we investigate directional residual stress distribution at the part scale (i.e. differences between the two in-plane stresses) of Ti-6Al-4V samples produced by LMD. The results in this work uncover additional directional residual stresses across the layers which is related to the alternating laser path in subsequent layers.

2. Material and methods

2.1 Sample production and preparation

The Ti-6Al-4V samples of this investigation were produced using the LMD AM process with a coaxial powder feed. LMD was carried out using a IPG fibre laser with outcoupling fibre with a diameter of 600 µm and a maximum power of 7 kW. The focal lens of 250 mm and collimator with a focal length of 125 mm result in a laser spot diameter of 1200 µm on the substrate. The specimens were built at a constant laser power of 500 W while the nozzle was moving at a linear scan speed of 1000 mm/min. The metal powder was fed into the melt pool created by the laser through a continuous coaxial nozzle (Fraunhofer—Institüt für Lasertechnik, Munich, Germany) using argon as transport and shielding gas. The transport gas flow rate varied between 6–8 L/min blowing 2.96 g/min Ti-6Al-4V particles into the melt pool. The contour of each layer was deposited first and then filled via a continuous bidirectional scan strategy with a spacing of 600 µm between neighbouring scan tracks. The layer thickness was 500 µm and the scanning direction of successive layers was rotated by an angle of 90°. Ti-6Al-

4V grade 5 alloy powder with a particle size of 45-100 µm was used. Samples were built on Ti-6Al-4V flat substrates with a thickness of 18 mm.

Figure 1 shows the geometry of the samples. The z orientation is always along the build direction (BD) and the other two coordinates (x and y) correspond to the laser scan directions that make up the layer plane. After production, the samples (XY, XY single and XZ) were removed from the substrate (Figure 1(a)) by wire Electrical Discharge Machining (EDM). Each of the larger XY and XZ samples were subdivided into four sections using wire EDM equipped with a 250 µm brass wire, each section was about 14.8 mm thick (Figure 1(b)). The effect of the sectioning on the measured residual stresses will be discussed later. The mechanical properties in two loading directions, vertical and horizontal, are shown in Table 1, as measured via tensile tests on flat, standard size "dogbone" shaped specimens according to E8M-16a. The samples were extracted from rectangular samples, the final shape was cut by wire EDM (gauge volume 6x3x32 mm^2), and deformations during tensile testing measured using a 25 mm gauge length extensometer. 'Horizontal' corresponds to loading along the layer plane, perpendicular to the BD, and 'vertical' to loading parallel to the BD. This data is later used in processing of the ICHD and slitting results.

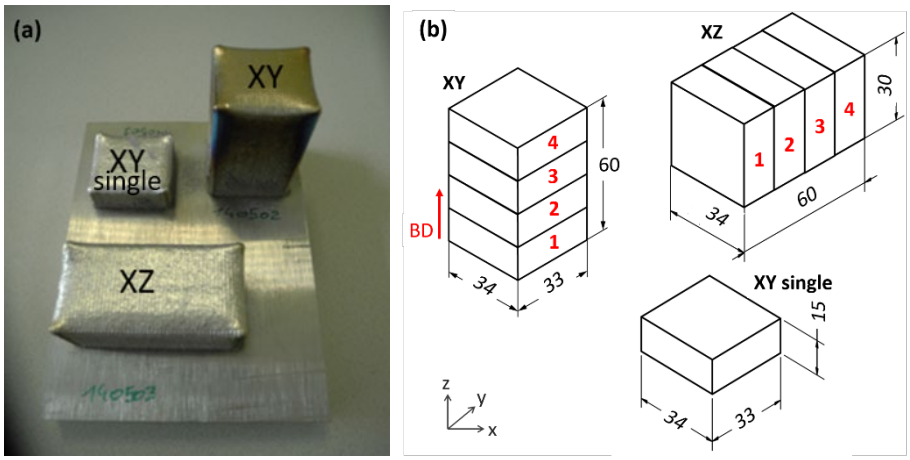

Figure 1: (a) Ti-6Al-4V laser metal deposited samples on the substrate and (b) schematic representation of the samples and the cuts made by EDM (dimensions in mm).

Table 1. Bulk material properties of laser metal deposited Ti-6Al-4V specimens obtained by static tensile testing. 'Horizontal' corresponds to loading along the layer plane, perpendicular to the build direction, and 'vertical' to loading parallel to the build direction.

Specimen	E [GPa]	σ_{yield} [MPa]	ε_f [%]	ν
Ti-6Al-4V (horizontal)	112.3 ± 1.4	1,022 ± 18.4	4 ± 1.4	0.31 ± 0.01
Ti-6Al-4V (vertical)	113.6 ± 2	830 ±11	13.9 ± 2.8	0.32 ± 0.01
Ti-6Al-4V (averaged)	113	926	9	0.315

2.2 Incremental centre hole drilling and slitting method

To capture the mesoscale residual stress variations, the measurements were performed using ICHD with precision milling system according to ASTM standard E837-13a [32]. A tungsten carbide inverted cone drill with a nominal diameter of 1.6 mm was used. To prepare for ICHD, soft grinding with 1200 grit sand paper was applied on the surfaces created by wire EDM to remove the recast layer and allow better adhesion of the strain rosettes. Strain gauge rosettes (CAE-06-062UL-120) were installed on both sides of each section. Figure 2(a) shows the schematic representation of the sections (XZ and XY) with the orientation of the layers and the strain gauge installation of the ICHD measurements.

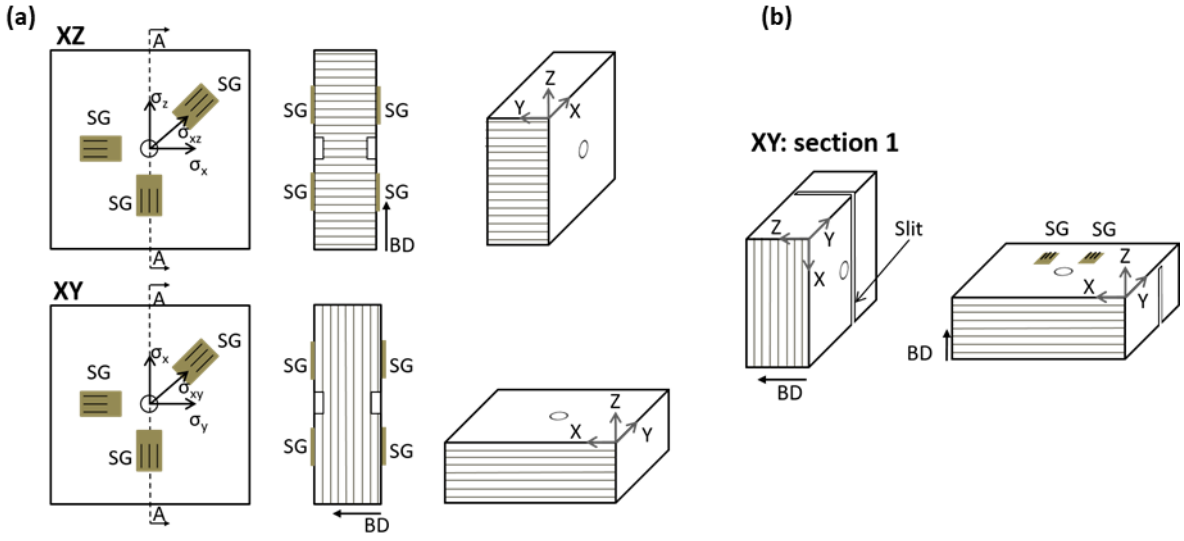

Figure 2: Schematic illustration of the installation of the strain gauge (SG) rosettes on the (a) XZ and XY sections from the case of the incremental centre hole drilling and (b) on the XY

section 1 that was subjected to the slitting process. The orientation of the layers is indicated in the 3D representations and the cross-sections.

During ICHD the strains were recorded in 50 μm increments of depth while the drilling speed was 0.07 mm/min. The drilling was performed creating holes of roughly 2 mm diameter. The final hole depth was 1 mm deep. After the ICHD process, the diameter of the drilled hole was measured by an optical microscope. The measured relaxed strains and the diameter of the holes were used to calculate the RS using the Internal Stress Instrumentation Software (ISIS) provided by VEQTER Ltd.. For all the cases, the stress along the BD corresponds to σ_z. In the case of XZ samples, the measured in-plane stress corresponds to the σ_z and σ_x. For the case of XY samples, the measured stresses correspond to the σ_x and σ_y.

Note that in ICHD, uncertainties such as the hole depth and eccentricity errors can be introduced in the results. Uncertainties in material properties could also potentially increase the errors, while the sensitivity of strain gauges decreases with increased depth [33]. The latter limitation is the main reason for the limited depth of the hole. When stresses are too high, localised plastic yielding in the region around the hole is a main contributor for the total uncertainty. According to the ASTM Standard E837-13a [32], depending on the thickness of the material, the measured residual stresses should not exceed 50% to 80% of the material yield stress. In this study, the residual stresses never exceed 30% of the yield stress (830 MPa).

In parallel with ICHD, the slitting method [28,29] was used to both independently verify the ICHD results and to see if mesoscale variations are present across multiple layers. Recent improvements in slitting have enabled the ability to resolve detailed stress variations on small length scales [34–36], although that resolution has never before been demonstrated over the length scale that was measured in this study. After the ICHD measurements, incremental slitting was performed in section 1 of the XY sample. Using a conventional arrangement for through-thickness measurements, two strain gauges were installed at the top of the sample,

which would be the face opposite of the slit. Figure 2(b) shows that the strain gage and slit locations were selected to minimize any effects from the drilled holes. The sample was slit using wire EDM with a 100 μm diameter brass wire and skim cut settings to minimize any EDM-induced stresses [37]. The slit cut was performed along the z direction (build direction) though the thickness of 14.78 mm, oriented to measure the in-plane σ_y.

Achieving mesoscale resolution though the whole part required pushing the state-of-the-art both experimentally and analytically for the slitting method. During the slitting, 10 cut increments per 0.5 mm thick layer would be ideal to oversample and allow calculation of the stress variations in the presence of experimental noise. For the 14.78 mm thick sample, that would give nearly 300 cut increments, an order of magnitude more than the 30-40 cuts commonly needed to resolve a macrostress profile in the presence of noise [38]. As a compromise with experimental time, the initial cut depth increments of 51 μm were doubled to 102 μm after about 8 build layers, doubled again after about 5 more layers, and then halved back to 102 μm for the final 7 layers. This cutting strategy resulted in 161 cut increments, still far more than has ever been reported for slitting.

Calculating stresses from the strain data requires solving an elastic inverse problem to account for the stress re-arrangement during the cutting [39]. Such solutions must smooth out noise effects in the data to accurately capture the physical results without amplifying data noise. Traditional series expansion methods for solving the inverse problem [29,40,41] lack the flexibility to resolve the mesoscale variations. Instead, the newer pulse regularization method [39], which has proven vastly superior for resolving complicated, localized stress variations [30,34,42] was applied. The calculations require a “compliance matrix” to relate RS to measured strain, and this was developed from a set of elastic finite element analyses customized to this sample, following a standard approach [43], and assuming plane strain conditions [44]. Uncertainties were estimated using strain error propagated through the inverse solution and

also uncertainty in the Tikhonov regularization parameter β [38]. This approach has been shown to capture the most significant sources of random uncertainty [38]. The most likely source of bias errors would be plasticity as the stresses rearrange during slitting. The methodology in [45] was applied and confirmed the lack of plasticity errors in these measurements.

In this work, we assume that elastic anisotropy due to texture does not have a significant effect on the stress calculation. Furthermore, although the stress relaxation from material removal is localized, the resulting strains are measured some distance from the hole or slit and are averaged over a finite size strain gauge. The strain gauge sets the scale over which the elastic properties are effectively averaged. Thus, it is appropriate to use the bulk elastic properties on both measurements. The RS of the XY and XZ specimens were calculated using the elastic constants of Table 1. The elastic constants of the horizontal loading direction were used for the XY specimen. For the XZ sections, the average value of both horizontal and vertical elastic constants was used for the calculations.

After the measurements, a Zeiss Axio Imager.M2m and an Axioskop 40A/40 Pol microscope was used to study the microstructure around the slit and the hole in order to relate the position of the layers to the measured RS profile. Samples were embedded in epoxy resin and ground using 1200 grit SiC paper, polished using a 0.25 μm SiO_2/ H_2O_2 suspension and etched for 5 seconds in a solution of 50 ml H_2O, 25 ml HNO_3 and 5 ml HF. Following the etching procedure, samples were left in a 10% boric acid solution overnight to neutralize leftover HF.

3. Results

3.1 ICHD: In-plane residual stresses of the XY and XZ individual sections

Figure 3(a) and (b) show the schematic representation of the XY sections and the single XY sample respectively. Figure 4 shows the schematic representation of the XZ sections. The

illustrated dashed lines indicate the regions where the samples were EDM cut and the grey planes specify the sides of the sections where the measurements took place. The RS distribution through the ICHD depth of 1 mm is shown for five representative sections of the XY sample in Figure 3(a) and for four representative sections for the XZ sample in Figure 4. Figure 3(b) shows the RS distribution of the two sides of the XY single sample. Throughout, σ_x, σ_y and σ_z are represented by blue, red and green markers respectively. The stresses are representative of the central location of each plane.

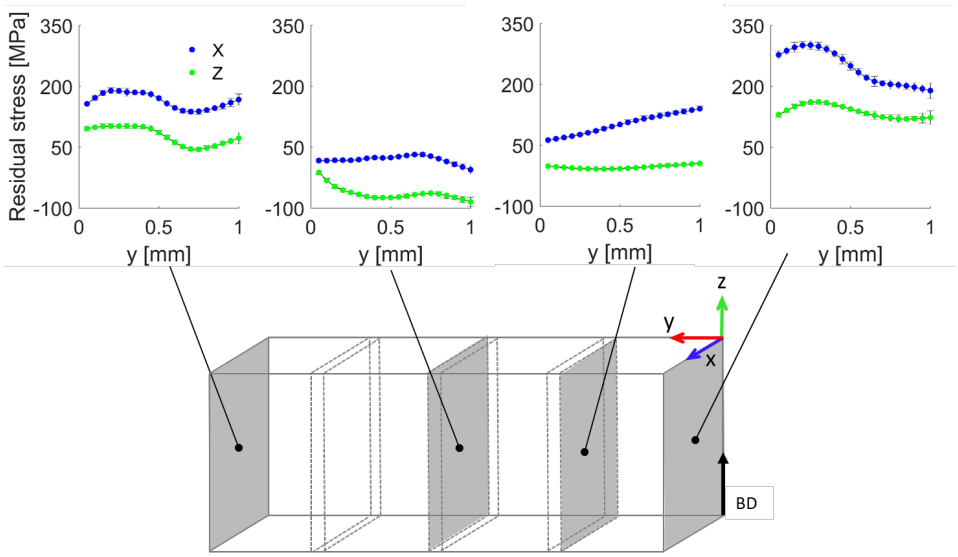

Figure 4: Schematic illustration of the sample geometry with representative graphs of the residual stress distribution as measured via incremental centre hole drilling (ICHD) along the 1 mm depth for the sections of the XZ sample. The grey planes indicate the sides where the representative graphs of the ICHD measurements took place and the dashed lines indicate the extracted sections.

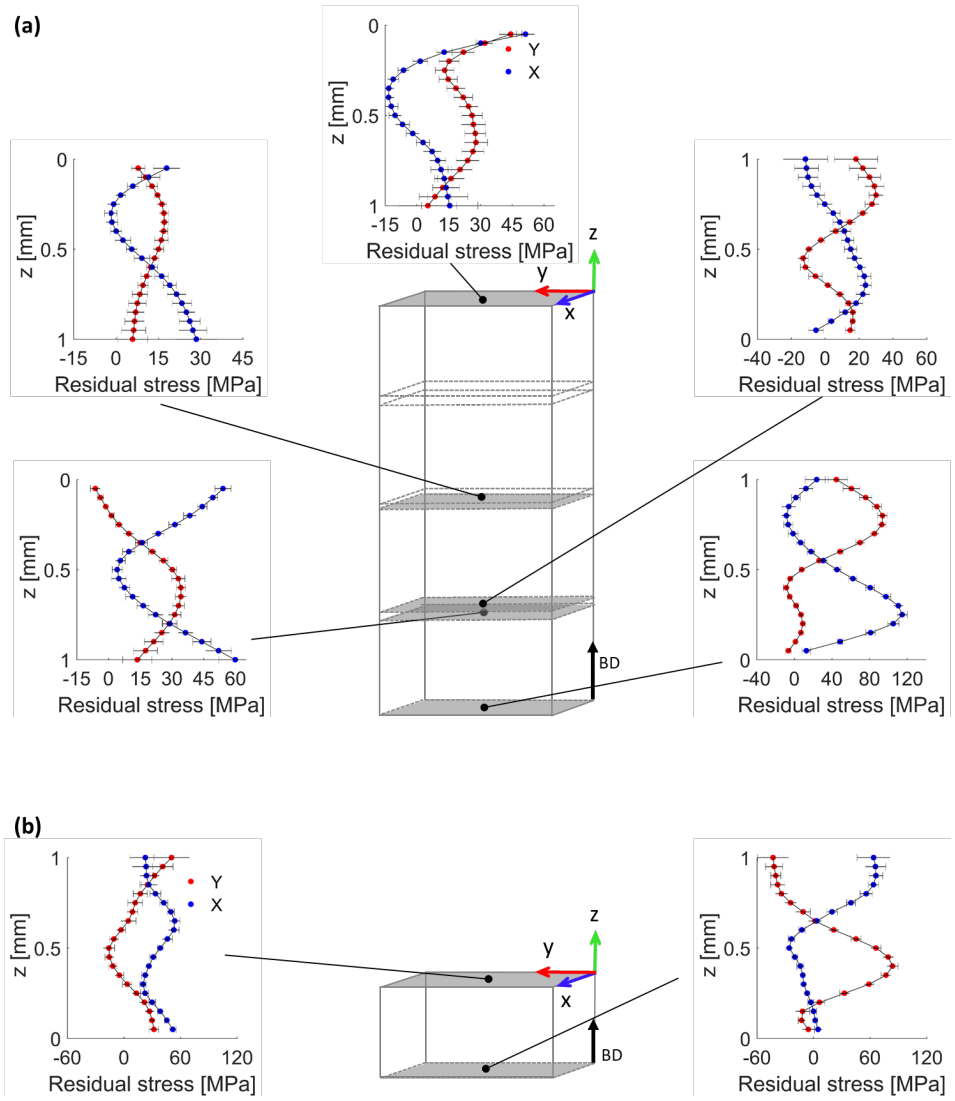

Figure 3: Schematic illustration of the sample geometry with representative graphs of the residual stress distribution as measured via incremental centre hole drilling (ICHD) method along the 1 mm depth of: (a) the sections of the XY sample and (b) the single XY sample. The dashed lines of (a) indicate the extracted sections. The sides where the representative graphs of the ICHD measurements took place are shown in grey and the build direction (BD) corresponds to the z stress component.

The XY sample indicates that the maximum RS (in-plane σ_x and σ_y) magnitude is present at section '1' extracted from the bottom (nearest the substrate) of the initial XY sample (120 MPa) while the sections that were extracted from positions closer to the top of the initial XY sample indicate lower residual stresses (between -15 and 60 MPa). Similar RS distribution was also observed at the single XY sample (see Figure 3(b)). Figure 4 shows the RS distribution of

the individual sections extracted from the XZ sample. Residual stresses ranging from -100 MPa to 330 MPa are present in the sections of the XZ sample. The highest tensile stresses exist at the free surfaces of the sample while the highest compressive stress (-100 MPa) is located in the middle of the sample.

A remarkable feature of all graphs of Figure 3(a) and Figure 3(b) is the mesoscale directional oscillatory RS variation in the x and y stresses. Notably, the oscillatory variations are significantly larger than the uncertainties. This variation was also observed in the measurements performed on the other XY sections that are not shown in the current paper. Moreover, when σ_x reaches a maximum, σ_y tends to be near its minimum, indicating strong directionality. On the other hand, for the XZ sample, the hole drilling direction is parallel to the layers rather than perpendicular and only macroscale stress variations are observed. Figure 4 shows that the horizontal σ_x is larger than the vertical σ_z on the extreme sides of the sample. Additionally, the σ_x and σ_z displayed similar behaviour as a function of drilling depth, in contrast to the σ_x and σ_y in the measurements of the XY sections.

3.2 Incremental slitting: y stress measurement through the thickness of an XY section

The slitting method was performed in section '1' of the XY sample (Figure 2(b)). Because the use of slitting to measure mesoscale stresses over such a long range was unproven, the raw strain data is examined in Figure 5 prior to stress calculation. The strains measured by the two gauges show a long-range trend into compression with slope changes over regions of several mm. The data also appear to show a finer length scale signal. To extract the finer scale signal, the data were fit using smoothing splines limited to macroscale variations on the order of several mm. The difference between the macroscale fits and the data are then plotted as misfits on the smaller strain scale on the right axis. These misfits show a very clear alternating signal with a wavelength of 1 mm, consistent with the ICHD results in Figure 3a. The peak-to-valley amplitude of this mesoscale signal range from a minimum of about 4 με to about 20 με at the

end of the cut, well above the 1 με resolution limit of the strain instrumentation. There is clearly a mesoscale oscillatory stress variation causing this aspect of the data.

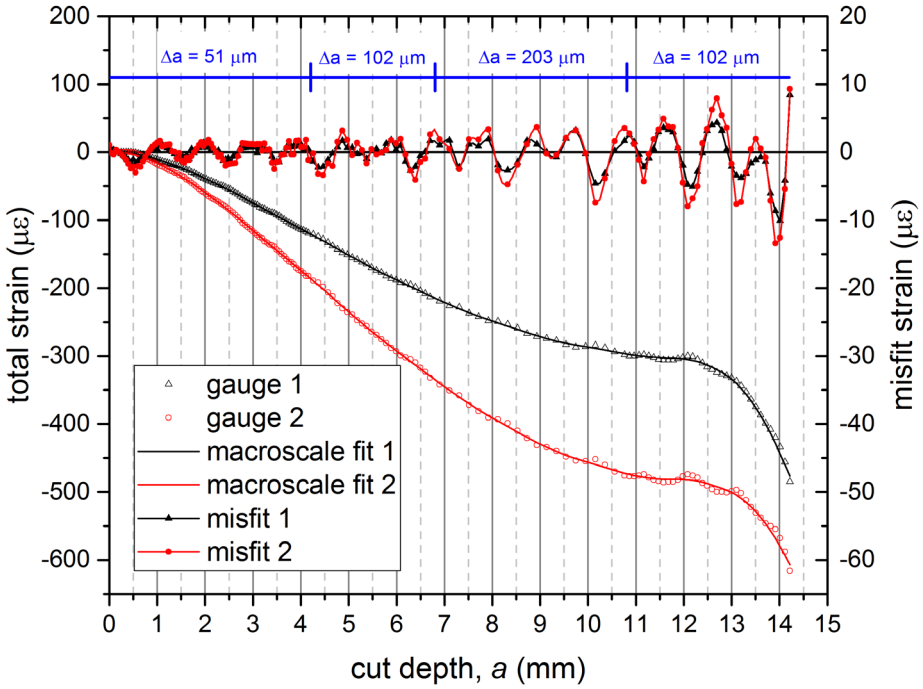

Figure 5: Through thickness strain profile of the section 1 of sample XY as determined by the slitting process.

The macroscale difference between the two strain gauges indicates that the residual stresses were not constant along the y direction of the sample (see Figure 2(b)). Considering the path dependent nature of the AM process, such variation is quite plausible. The data from each gauge was analysed separately to provide an indication of that variation.

Figure 6 shows the slitting results of σ_y as a function of the first 4 mm along the thickness of the section 1 of the XY sample. It is apparent that the alternating signal with a wavelength of 1 mm previously observed in the ICHD measurements is also observed in the slitting RS distribution of σ_y (see Figure 6), but now over the depth of about eight build layers. As with the ICHD measurements, the oscillations are significantly larger than the uncertainties. As previously mentioned, the increment size of the ICHD measurements was 50 μm while the increment size of the slitting was 51 μm only for the first 4 mm. The full depth slitting results, including the lower resolution regions, will be presented in the next section. In Figure 6, the

directional residual stresses (σ_x and the σ_y) of the ICHD measurements for the same sample are also shown. It can be seen, that the σ_y results of the ICHD measurements are in good agreement with the σ_y results of the slitting measurements, with the magnitudes falling between the two slitting results from slightly different locations. The small z offset between the hole drilling and slitting results may be caused by different surface preparation and by experimental uncertainties in the initial cut/hole depth.

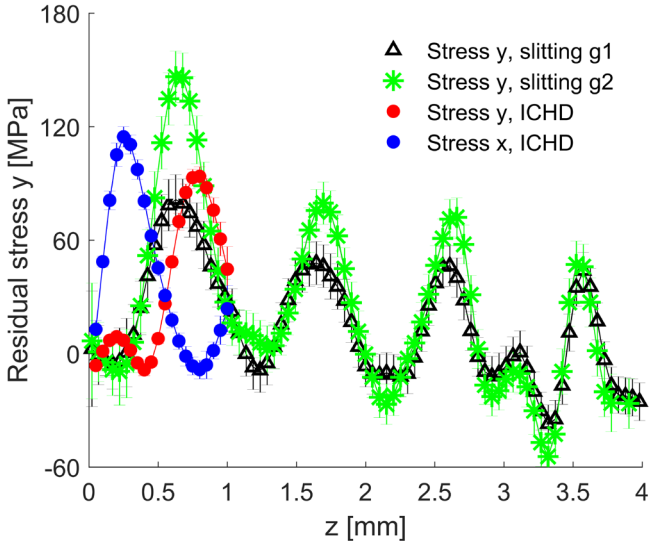

Figure 6: Residual stress as a function of depth over the first 4 mm along the thickness of the section 1 of the XY sample. Slitting g1 and g2 respectively correspond to strain gauge 1 and gauge 2 used for slitting.

4. Discussion

4.1 Effect of sectioning on interpretation of measured residual stresses

The RS that are built up in a component during manufacturing should attain equilibrium between tensile and compressive stresses. Accordingly, the macroscale tensile stresses on the outer surfaces must be balanced by compressive stresses in the centre.

The cuts used to section the specimen prior to ICHD and slitting certainly perturbed the stresses in a region near the cut. Had the sectioning cuts been used for a contour method RS measurement, the change in the stresses could have been determined [34,46]. Nonetheless, such effects are well understood [47,48] and are expected to have minimal effect on the

interpretation of mesoscale in-plane stress variations. Since the proof by Bueckner [49], it has long been understood that the *change* in all residual stress components from a cut is entirely determined by the stresses that existed on the plane of the cut and only the stresses with a component normal to the cut (e.g., σ_z, τ_{xz}, and τ_{yz} for a cut with normal in the z-direction, the ones that are fully relaxed on the cut plane). Pagliaro *et al.* shows in [46] that the sectioning effect on all stress components is localized to a region near the cut, in accord with St. Venant's principle[1]. The extent of the affected region is largest for longer-wavelength stress variations and smaller for shorter-range stress variations [47] and the stress change will generally smooth out stress variations as it decays away from the surface.

Therefore, importantly, a macrostress distribution released by the cut could not alter the mesoscale stress variation. Any mesoscale stresses observed post-sectioning had to exist prior to sectioning. Longer range stress variations, such as the background parabolic distribution over the whole range, are likely changed by the sectioning.

4.2 Effect of the build layers and the scanning direction on the in-build-plane residual stresses

The results of Figure 3(a), highlight that the height of the sample influences the RS distribution, as was also discussed in Ref. [7,50]. In the case of the single sample, the top measurements correspond to a location approximately 30 layers above the substrate, while in the larger XY sample the top of section 4 corresponds to a location approximately 120 layers above the substrate. As mentioned in section 3.1, the highest RS is located near the bottom. Moving from the bottom to the top, the magnitude of the stress decreases. The cooling rate for a layer high up in the sample is lower than that for the first layers [51]. During deposition of the first layers, the base plate, which acts as a heat sink, is at room temperature and in close proximity to the deposition. Thus, cooling rates are high. As the build progresses and the part

[1] For further clarity, the reader is referred to Figure 2 of the referenced article [46].

becomes taller, the base plate warms up considerably and gets farther from the deposition, reducing the temperature differential and the thermal conductivity. As a result, the cooling rate is significantly lower when depositing at the top of the build. Observationally, this manifests as a considerably longer visual afterglow when depositing layers near the top, than during deposition of layers near the substrate. Consequently, the temperature gradients and cooling rates are smaller near the top, resulting in lower residual stresses.

The directional oscillatory variation of the σ_x and σ_y of Figure 3(a) and (b) was present every 1 mm, meaning that the distance between a maximum and minimum for a particular stress direction is roughly 0.4 to 0.5 mm. The sinusoidal trend is more pronounced for the sections with higher stress magnitudes (see the two graphs of the bottom section of Figure 3(a)). The slitting measurements also indicated an oscillatory behaviour of the σ_y with a periodicity of 1 mm, i.e. the distance between a maximum and minimum is 0.5 mm. This behaviour of the stress in each direction is offset with respect to each other, indicating that the σ_x and σ_y oscillate out of phase with each other. Those crossovers are present only in the XY samples where the ICHD and slitting measurements were conducted perpendicular to the layers.

Figure 7 shows micrographs of the cross-section through both holes in the single XY sample. The dashed lines on the sides of the micrographs represent the layer boundaries, which are made visible in the microstructure due to a small heat affected zone (HAZ). It is revealed that the micrographs and the directional residual stress oscillations match the layers of the sample. The micrograph from the top of the single XY sample is shown in Figure 7(a). The σ_y (shown in red) reached the minimum value (-16 MPa) on the boundary of layers 1 and 2 and approaches a maximum of 50 MPa near the final hole depth of 1 mm. On the other hand, the σ_x appears to peak somewhere inside the layers. Similar results are observed also in Figure 7(b) where the cross section of the sample's bottom part is depicted. The exact location of the maxima and

minima in the RS distribution with respect to the layer boundaries is determined by the initial RS creation due to the deposition of a layer, but also by the thermal cycles induced by deposition of subsequent layers. These cycles lead to partial remelting of a layer and may induce stress relief in the HAZ. The exact influence thereof is unknown, but the results in this paper suggest that the layer boundary is still the most likely location for the local maxima and minima in the RS distribution.

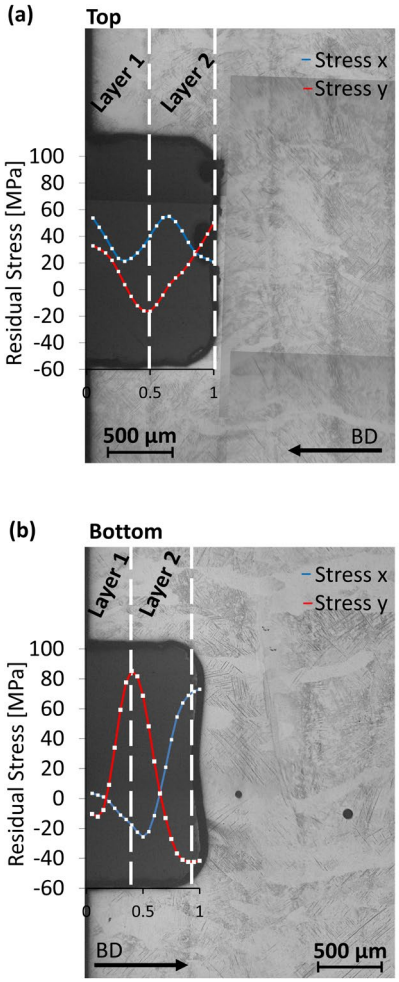

Figure 7: Micrographs of the single XY sample and the ICHD residual stress distribution for the (a) top and (b) bottom of the section. The white dashed lines indicate the layer boundaries.

As previously mentioned, the scanning direction was rotated 90° for every layer. The presented results indicate that the σ_y periodically reaches a maximum at the bottom of a layer that was scanned in the Y direction, while the same is true for the σ_x and layers scanned in the

X direction. The maxima are offset by one layer thickness, and each minimum of the stress in one direction coincides with a maximum of the stress in the other direction. It is widely known from the literature that the stress in the direction of the scan vectors is always larger than the stress perpendicular to the vectors [13,52–54]. Gusarov et al. [52], for example, postulated that the stresses parallel to the scan vectors are about twice as high as those perpendicular to them. One of the main reasons of this directionality is the constraints that are acting on the scan vector during shrinkage. The solid material of the previously deposited layers beneath it restricts the longitudinal contraction of the scan vector. A similar effect is also taking place for the transverse contraction; however, the transverse contraction is considerably smaller due to the dimensional aspect ratio of the newly deposited material and the fact that the material is only restricted on one side by the previously deposited scan vector. For the first time, this paper confirms that the directional residual stresses within one layer persists in Ti-6Al-4V LMD samples despite the deposition of additional layers (and their associated HAZ) on top.

In Figure 8(a) the RS distribution of the full thickness of section 1 of the XY sample (14.7 mm) is presented. The through-thickness slitting measurement in Figure 8 of the σ_y through nearly 30 layers shows that the mesoscale stress variations persist throughout the sample, which confirms and extends the ICHD results through only the first two layers near the EDM cut surfaces. To match the RS profile with the actual layer locations, the RS graphs are shown on the top of micrographs of the cross-section of the sample. The BD and the slitting cut direction (SD) are indicated on both illustrations. The increment size of the slitting cut along the thickness of the sample is indicated as Δa. Despite the poorer spatial resolution in regions with larger cut increments, the stresses reveal the same mesoscale oscillatory variation that was observed in the case of the ICHD measurements. A more detailed plot of the first 4 mm where the slitting increment cut was (51 μm) is shown in Figure 8(b). The grey dots indicate the y-oriented layers with an out-of-plane scan direction, in which the crescent-shaped

melt pools are visible. It is apparent from Figure 8(b) that the σ_y is reaching the maximum tensile value at the bottom of the y oriented layers.

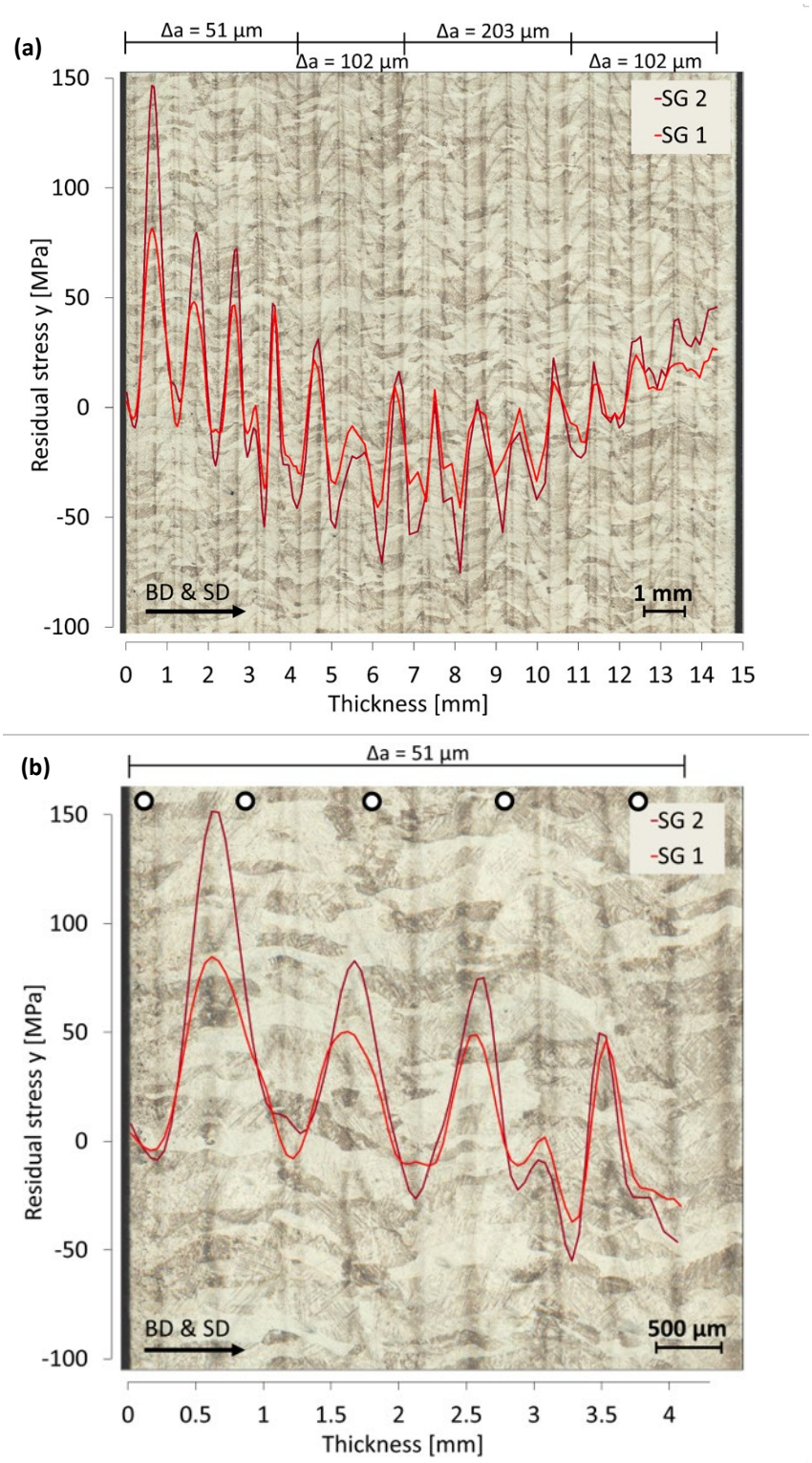

Figure 8: Micrographs of the cross-sections of the section 1 of the XY sample and the residual stress distribution of the y stress component as determined by the slitting process. In (a) the full thickness of the sample (14.7 mm) is shown and in (b) a higher resolution micrograph of the first 4 mm of the sample's thickness is presented. The build direction (BD) and the slitting

cut direction (SD) are also shown on the illustrations and grey dots correspond to the y-oriented layers. The residual stress uncertainties are between ± 5-30 MPa.

Overall, the stress profiles indicate significant variations across the interface of each subsequent layer. Even though the addition of new layers affects the stress state within one layer by effectively thermally cycling the previous layer, this research provides strong evidence that the local mesoscale directional residual stresses survives that deposition of subsequent layers and the associated thermal and plastic effects. This is important for local crack growth behaviour in cyclically loaded applications because localized stress risers provide likely nucleation points for crack formation. Although that literature indicates that the HAZ does not significantly affect the crack initiation in titanium welded joints [55], the presence of the maximum stress at the HAZ can affect the crack nucleation. The results indicate that the maxima in the stress coincides with the laser track direction which is also consistent with the literature [4],[13,56–60].

Moreover, these results are particularly important for the development of predictive computational models. The current results suggest that localized temporal and spatial gradients in temperature within a single layer might be needed in the assumptions of computational models in order to predict mesoscale residual stresses. Recent efforts to model the residual stress development during AM based upon adding a full layer of material at a time [61–63] are inherently unable to predict the extreme spatial gradients in temperature and residual stresses within a single layer.

5. Conclusions

The directional mesoscale residual stress distributions in additively manufactured Ti-6Al-4V components produced by laser metal deposition (LMD) process were investigated by means of incremental centre hole drilling and the slitting method. Using two complementary measurement techniques allowed broader insight into the stress state. Note that the use of these

well-established methods for the characterization of the mesoscale residual stresses support the fidelity of the novel findings of this article. Incremental centre hole drilling revealed the out of phase sinusoidal behaviour of the x and y build-plane stress components and showed a mesoscale directional oscillatory variations over two near-surface layers. Conversely, slitting showed that the mesoscale oscillatory variations persist across the entire part. The maximum stresses within a layer are found near the bottom of that layer, parallel to the scan direction. Combined, the results show that directional intra-layer residual stresses induced by the deposition pattern persisted during deposition of subsequent layers. The presented results can be used to provide essential insight on the mesoscale directional residual stress distribution in Ti-6Al-4V parts produced by LMD that would be of high importance for computational models of the AM process and for prediction of critical material behaviours such as crack growth rates, crack paths, and delamination. Future work will focus on the effect of various scan strategies on the mesoscale residual stresses. Certainly, those investigations can be accompanied by experimental results on crack growth behaviour as well as investigations on parts with complex geometries. With respect to the methods, future measurements could use more sophisticated approaches to account for the sectioning used to access internal stresses [34,46]. The slitting measurements could be repeated without sectioning and still access the internal mesoscale stress variations.

Acknowledgments

Research funded by an SBO Project grant 110070: eSHM with AM of the Agency for Innovation by Science and Technology (IWT), as well as an individual IWT grant number 121186. The authors would like to thank Dr. Bjørn Clausen, Dr. Ed Kingston, Dr. Xavier Ficquet, Mr. Ian Lewsey and Mr. Ramon M. Martinez for their kind assistance during the measurements and their valuable feedback. Part of this work was performed under the auspices of the U.S. Department of Energy by Los Alamos National Laboratory under contract DE-

AC52-06NA25396, and by Lawrence Livermore National Laboratory under Contract No. DE-AC52-07NA27344.

References

[1] ASTM International, F2792-12a: Standard Terminology for Additive Manufacturing Technologies, (2003). doi:10.1520/C0033-03.

[2] D.D. Gu, W. Meiners, K. Wissenbach, R. Poprawe, Laser additive manufacturing of metallic components: materials, processes and mechanisms, Int. Mater. Rev. 57 (2012) 133–164. doi:10.1179/1743280411Y.0000000014.

[3] R.J. Moat, A.J. Pinkerton, L. Li, P.J. Withers, M. Preuss, Residual stresses in laser direct metal deposited Waspaloy, Mater. Sci. Eng. A. 528 (2011) 2288–2298. doi:10.1016/j.msea.2010.12.010.

[4] P. Mercelis, J.-P. Kruth, Residual stresses in selective laser sintering and selective laser melting, Rapid Prototyp. J. 12 (2006) 254–265. doi:10.1108/13552540610707013.

[5] M. Geiger, F. Vollertsen, The Mechanisms of Laser Forming, CIRP Ann. - Manuf. Technol. 42 (1993) 301–304. doi:10.1016/S0007-8506(07)62448-2.

[6] M.P. Mughal, R.A. Mufti, H. Fawad, The mechanical effects of deposition patterns in welding-based layered manufacturing, Proc. Inst. Mech. Eng. Part B J. Eng. Manuf. 221 (2007) 1499–1509. doi:10.1243/09544054JEM783.

[7] P. Rangaswamy, M.L. Griffith, M.B. Prime, T.M. Holden, R.B. Rogge, J.M. Edwards, R.J. Sebring, Residual stresses in LENS components using neutron diffraction and contour method, Mater. Sci. Eng. A. 399 (2005) 72–83. doi:10.1016/j.msea.2005.02.019.

[8] P. Rangaswamy, T.M. Holden, R.B. Rogge, M.L. Griffith, Residual stresses in components formed by the laserengineered net shaping (LENS) process, J. Strain Anal. Eng. Des. 38 (2003) 519–527. doi:10.1243/030932403770735881.

[9] S. Ghosh, J. Choi, Deposition Pattern Based Thermal Stresses in Single-Layer Laser Aided Direct Material Deposition Process, J. Manuf. Sci. Eng. 129 (2007) 319. doi:10.1115/1.2401620.

[10] P. Aggarangsi, J.L. Beuth, M. Griffith, Melt Pool Size and Stress Control for Laser-Based Deposition Near a Free Edge, Proc. 14th Solid Free. Fabr. Symp. (2003) 196–207.

[11] K. Zhang, S. Wang, W. Liu, R. Long, Effects of substrate preheating on the thin-wall part built by laser metal deposition shaping, Appl. Surf. Sci. 317 (2014) 839–855. doi:10.1016/j.apsusc.2014.08.113.

[12] P. Pratt, S.D. Felicelli, L. Wang, C.R. Hubbard, Residual Stress Measurement of Laser-Engineered Net Shaping AISI 410 Thin Plates Using Neutron Diffraction, Metall. Mater. Trans. A. 39 (2008) 3155–3163. doi:10.1007/s11661-008-9660-9.

[13] A.H. Nickel, D.M. Barnett, F.B. Prinz, Thermal stresses and deposition patterns in layered manufacturing, Mater. Sci. Eng. A. 317 (2001) 59–64. doi:10.1016/S0921-5093(01)01179-0.

[14] M.L. Griffith, M.E. Schlienger, L.D. Harwell, M.S. Oliver, M.D. Baldwin, M.T. Ensz, M. Essien, J. Brooks, C. V. Robino, J.E. Smugeresky, W.H. Hofmeister, M.J. Wert, D. V. Nelson, Understanding thermal behavior in the LENS process, Mater. Des. 20 (1999) 107–113. doi:10.1016/S0261-3069(99)00016-3.

[15] E.R. Denlinger, J.C. Heigel, P. Michaleris, Residual stress and distortion modeling of electron beam direct manufacturing Ti-6Al-4V, Proc. Inst. Mech. Eng. Part B J. Eng. Manuf. (2014) 0954405414539494-. doi:10.1177/0954405414539494.

[16] N. Shamsaei, A. Yadollahi, L. Bian, S.M. Thompson, An Overview of Direct Laser Deposition for Additive Manufacturing; Part II: Mechanical Behavior, Process Parameter Optimization and Control, Addit. Manuf. 8 (2015) 12–35. doi:10.1016/j.addma.2015.07.002.

[17] S. Zhang, X. Lin, J. Chen, W. Huang, Influence of heat treatment on residual stress of Ti-6Al-4V alloy by laser solid forming, Rare Met. Mater. Eng. 38 (2009) 774–778. doi:1002-185X(2009)05-0774-05.

[18] L.M. Sochalski-Kolbus, E.A. Payzant, P.A. Cornwell, T.R. Watkins, S.S. Babu, R.R. Dehoff, M. Lorenz, O. Ovchinnikova, C. Duty, Comparison of Residual Stresses in Inconel 718 Simple Parts Made by Electron Beam Melting and Direct Laser Metal Sintering, Metall. Mater. Trans. A Phys. Metall. Mater. Sci. 46 (2015) 1419–1432. doi:10.1007/s11661-014-2722-2.

[19] M. Strantza, R.K. Ganeriwala, B. Clausen, T.Q. Phan, L.E. Levine, D. Pagan, W.E. King, N.E. Hodge, D.W. Brown, Coupled experimental and computational study of residual stresses in additively manufactured Ti-6Al-4V components, Mater. Lett. 231 (2018) 221–224. doi:10.1016/j.matlet.2018.07.141.

[20] H. Ali, H. Ghadbeigi, K. Mumtaz, Effect of scanning strategies on residual stress and mechanical properties of Selective Laser Melted Ti6Al4V, Mater. Sci. Eng. A. 712 (2018) 175–187. doi:10.1016/j.msea.2017.11.103.

[21] L. Parry, I.A. Ashcroft, R.D. Wildman, Understanding the effect of laser scan strategy on residual stress in selective laser melting through thermo-mechanical simulation, Addit. Manuf. 12 (2016) 1–15. doi:10.1016/j.addma.2016.05.014.

[22] J.H. Robinson, I.R.T. Ashton, E. Jones, P. Fox, C. Sutcliffe, The effect of hatch angle rotation on parts manufactured using selective laser melting, Rapid Prototyp. J. (2018) RPJ-06-2017-0111. doi:10.1108/RPJ-06-2017-0111.

[23] P.J.J. Withers, H.K.D.H.K.D.H. Bhadeshia, Residual stress Part 1 – Measurement techniques, Mater. Sci. Technol. 17 (2001) 355–365. doi:10.1179/026708301101509980.

[24] P.J. Withers, H.K.D.H. Bhadeshia, Residual stress. Part 2 – Nature and origins, Mater. Sci. Technol. 17 (2001) 366–375. doi:10.1179/026708301101510087.

[25] D. Stefanescu, C.E. Truman, D.J. Smith, P.S. Whitehead, Improvements in Residual Stress Measurement by the Incremental Centre Hole Drilling Technique, Exp. Mech. 46 (2006) 417–427. doi:10.1007/s11340-006-7686-8.

[26] G.S. Schajer, Measurement of non-uniform residual stresses using the hole drilling method - part I: Stress calculation procedure, Am. Soc. Mech. Eng. Mater. Div. MD. 7 (1988) 85–91. pas dispo online, ◆ partir 1990.

[27] G.S. Schajer, Measurement of non-uniform residual stresses using the hole drilling method. Part II. Practical application of the Integral method., J. Eng. Mater. Technol. - ASME. 110(4) (1988) 344–349.

[28] M.R. Hill, The Slitting Method, in: G.S. Schajer (Ed.), Pract. Residual Stress Meas. Methods, John Wiley & Sons, Ltd, 2013: pp. 89–108. doi:10.1002/9781118402832.ch4.

[29] W. Cheng, I. Finnie, Residual Stress Measurement and the Slitting Method, Springer Science+Business Media, LLC, New York, NY, USA, 2007.

[30] M.B. Prime, D.L. Crane, Slitting Method Measurement of Residual Stress Profiles, Including Stress Discontinuities, in Layered Specimens, in: M. Rossi, M. Sasso, N. Connesson, R. Singh, A. DeWald, D. Backman, P. Gloeckner (Eds.), Residual Stress. Thermomechanics Infrared Imaging, Hybrid Tech. Inverse Probl. Vol. 8, Conf. Proc. Soc. Exp. Mech. Ser., Springer International Publishing, 2014: pp. 93–102. doi:10.1007/978-3-319-00876-9_12.

[31] D.W. Brown, J.D. Bernardin, J.S. Carpenter, B. Clausen, D. Spernjak, J.M. Thompson, Neutron diffraction measurements of residual stress in additively manufactured stainless steel, Mater. Sci. Eng. a-Structural Mater. Prop. Microstruct. Process. 678 (2016) 291–298. doi:10.1016/j.msea.2016.09.086.

[32] ASTM, Determining Residual Stresses by the Hole-Drilling Strain-Gage Method, Stand. Test Method E837-13a. i (2008) 1–16. doi:10.1520/E0837-13A.2.

[33] G.S. Schajer, E. Altus, Stress calculation error analysis for incremental hole-drilling residual stress measurements, J. Eng. Mater. Technol. Asme. 118 (1996) 120–126. doi:10.1115/1.2805924.

[34] W. Wong, M.R. Hill, Superposition and Destructive Residual Stress Measurements, Exp. Mech. 53 (2013) 339–344. doi:10.1007/s11340-012-9636-y.

[35] M.B. Prime, M.R. Hill, Measurement of Fiber-Scale Residual Stress Variation in a Metal-Matrix Composite, J. Compos. Mater. 38 (2004) 2079–2095.

[36] M. Kerr, M.R. Hill, M.D. Olson, Study of Residual Stresses in Compact Tension Specimens Fabricated from Weld Metal, CORROSION. 69 (2013) 975–985. doi:10.5006/0832.

[37] W. Cheng, I. Finnie, M. Gremaud, M.B. Prime, Measurement of near-surface residual-stresses using electric-discharge wire machining, J. Eng. Mater. Technol. ASME. 116 (1994) 1–7.

[38] M.B. Prime, M.R. Hill, Uncertainty, Model Error, and Order Selection for Series-Expanded, Residual-Stress Inverse Solutions, J. Eng. Mater. Technol. 128 (2006) 175–185.

[39] G.S. Schajer, M.B. Prime, Use of Inverse Solutions for Residual Stress Measurements, J. Eng. Mater. Technol. 128 (2006) 375–382.

[40] G.S. Schajer, Application of finite element calculations to residual stress measurements, J. Eng. Mater. Technol. 103 (1981) 157–163.

[41] W. Cheng, I. Finnie, A method for measurement of axisymmetric axial residual stresses in circumferentially welded thin-walled cylinders, J. Eng. Mater. Technol. 107 (1985) 181–185.

[42] M.R. Hill, J.E. VanDalen, M.B. Prime, Assessment of Residual Stress in Fracture Mechanics Coupons, in: ASME Press. Vessel. Pip. Conf., Baltimore, Maryland, USA, 2011: pp. 421–426. doi:10.1115/pvp2011-57768.

[43] M.R. Hill, W.Y. Lin, Residual stress measurement in a ceramic-metallic graded material, J. Eng. Mater. Technol. 124 (2002) 185–191.

[44] C.C. Aydiner, M.B. Prime, Three-Dimensional Constraint Effects on the Slitting Method for Measuring Residual Stress, J. Eng. Mater. Technol. 135 (2013) 31001–31006. doi:10.1115/1.4023849.

[45] M.B. Prime, Plasticity effects in incremental slitting measurement of residual stresses, Eng. Fract. Mech. 77 (2010) 1552–1566. doi:10.1016/j.engfracmech.2010.04.031.

[46] P. Pagliaro, M.B. Prime, J.S. Robinson, B. Clausen, H. Swenson, M. Steinzig, B. Zuccarello, Measuring Inaccessible Residual Stresses Using Multiple Methods and Superposition, Exp. Mech. 51 (2011) 1123–1134. doi:10.1007/s11340-010-9424-5.

[47] J. Altenkirch, A. Steuwer, M.J. Peel, P.J. Withers, The extent of relaxation of weld residual stresses on cutting out cross-weld test-pieces, Powder Diffr. 24 (2012) S31–S36. doi:10.1154/1.3152580.

[48] W. Jiang, W. Woo, G.-B. An, J.-U. Park, Neutron diffraction and finite element modeling to study the weld residual stress relaxation induced by cutting, Mater. Des. 51 (2013) 415–420. doi:https://doi.org/10.1016/j.matdes.2013.04.053.

[49] H.F. Bueckner, The propagation of cracks and the energy of elastic deformation, Trans.

Am. Soc. Mech. Eng. 80 (1958) 1225–1230.

[50] C. Casalova, S.L. Campanelli, C. Pappaletere, Experimental analysis of residual stresses in the selective laser melting process, in: Proc. XIth Int. Congr. Expo., Florida, 2008.

[51] L. Wang, S. Felicelli, Y. Gooroochurn, P.T. Wang, M.F. Horstemeyer, Optimization of the LENS®process for steady molten pool size, Mater. Sci. Eng. A. 474 (2008) 148–156. doi:10.1016/j.msea.2007.04.119.

[52] A. V. Gusarov, M. Pavlov, I. Smurov, Residual stresses at laser surface remelting and additive manufacturing, Phys. Procedia. 12 (2011) 248–254. doi:10.1016/j.phpro.2011.03.032.

[53] M.F. Zaeh, G. Branner, Investigations on residual stresses and deformations in selective laser melting, Prod. Eng. 4 (2010) 35–45. doi:10.1007/s11740-009-0192-y.

[54] B. Cheng, S. Shrestha, K. Chou, Stress and deformation evaluations of scanning strategy effect in selective laser melting ☪, Addit. Manuf. 12 (2016) 240–251. doi:10.1016/j.addma.2016.05.007.

[55] C. Casavola, C. Pappalettere, F. Tattoli, Experimental and numerical study of static and fatigue properties of titanium alloy welded joints, Mech. Mater. 41 (2009) 231–243. doi:10.1016/j.mechmat.2008.10.015.

[56] M.F. Zaeh, G. Branner, Investigations on residual stresses and deformations in selective laser melting, Prod. Eng. 4 (2010) 35–45. doi:10.1007/s11740-009-0192-y.

[57] H. Pohl, A. Simchi, M. Issa, H.C. Dias, Thermal Stresses in Direct Metal Laser Sintering, in: Proc. Solid Free. Fabr. Symp., 2001: pp. 366–372.

[58] P. Mercelis, J.-P. Kruth, Residual stresses in selective laser sintering and selective laser melting, Rapid Prototyp. J. 12 (2006) 254–265. doi:10.1108/13552540610707013.

[59] J.-P. Kruth, J. Deckers, E. Yasa, R. Wauthle, Assessing and comparing influencing factors of residual stresses in selective laser melting using a novel analysis method, Proc. Inst. Mech. Eng. Part B J. Eng. Manuf. 226 (2012) 980–991. doi:10.1177/0954405412437085.

[60] B. Vrancken, R. Wauthle, J. Kruth, J. Van Humbeeck, Study of the influence of material properties on residual stress in selective laser melting, in: Proc. Solid Free. Fabr. Symp. Solid Free. Fabr. Symp., Austin, Texas, USA, 2013: pp. 1–15.

[61] T. Mukherjee, W. Zhang, T. DebRoy, An improved prediction of residual stresses and distortion in additive manufacturing, Comput. Mater. Sci. 126 (2017) 360–372. doi:10.1016/j.commatsci.2016.10.003.

[62] N.E. Hodge, R.M. Ferencz, J.M. Solberg, Implementation of a thermomechanical model for the simulation of selective laser melting, Comput. Mech. 54 (2014) 33–51. doi:10.1007/s00466-014-1024-2.

[63] M. Stender, L. Beghini, M. Veilleux, S. Subia, J. Sugar, Thermal Mechanical Finite Element Simulation of Additive Manufacturing: Process Modeling of the Lens Process, in: ASME. ASME Press. Vessel. Pip. Conf., 2017.